Supplemental Text

Generation and Characterization of Single and Compound FoxO Mutant Mice Reveals Modest Neoplastic Phenotypes. Each conditional allele retained wild type function as evidenced by normal FoxO expression and lack of a phenotype in homozygous mice and derivative cells (Supplemental Figures S1 and S2, and (Castrillon et al., 2003), see below; data not shown). Germline Cre-mediated recombination produced null alleles for each of the *FoxO* genes as confirmed by PCR, Southern, and Northern blot analyses (Supplemental Figures S1 and S2). Consistent with previous reports, *FoxO1* nullizygosity resulted in embryonic lethality *circa* E10.5, while *FoxO1*$^{-/+}$ mice were healthy and fertile (Furuyama et al., 2004; Hosaka et al., 2004). *FoxO3*$^{-/-}$ mice were viable and outwardly normal but developed mild hemolytic anemia, modest glucose intolerance, and premature female sterility due to global activation of primordial follicles soon after birth, as previously reported (Castrillon et al., 2003; Hosaka et al., 2004). Mice deficient for *FoxO4* were healthy and fertile with normal body weight and glucose tolerance (data not shown).

Each allele was backcrossed 3 times onto the FVBn background, after which serial intercrosses generated various experimental cohorts comprised of single and compound germline mutant mice (*FoxO3*$^{-/-}$*; FoxO4*$^{-/-}$ and *FoxO1*$^{-/+}$; *FoxO3*$^{-/-}$; *FoxO4*$^{-/-}$), triple conditional *FoxO1*$^{L/L}$; *FoxO3*$^{L/L}$; *FoxO4*$^{L/L}$ mice with and without the interferon-inducible Mx-Cre transgene (Kuhn et al., 1995), and wild type littermate controls. Overall survival as well as spontaneous and carcinogen-induced tumor formation was monitored in the various cohorts.

In the germline mutant series, aging *FoxO1*$^{+/+}$ and *FoxO1*$^{-/+}$ mice (n=31 and 52, respectively) showed no differences in overall survival, tumor incidence and multiplicity (*FoxO1*$^{+/+}$ = 0.9 ± 0.1 versus *FoxO1*$^{-/+}$ = 0.9 ± 0.1 tumors per mouse), and tumor spectrum (primarily lung adenocarcinomas which are common neoplasms in aged FVBn animals) (Supplemental Table S1 and Figure S3a). Similarly, aging *FoxO4*$^{+/+}$ and *FoxO4*$^{-/-}$ mice (n=26 and 37, respectively) failed to exhibit significant differences in overall survival, tumor incidence and multiplicity (*FoxO4*$^{+/+}$, 0.7 ± 0.1; *FoxO4*$^{-/-}$, 1.0 ± 0.2 tumors per mouse), and tumor spectrum (Supplemental Figure S3b, and Table S1). While aged FVBn females are reported to develop occasional prolactinomas (Mahler et al., 1996; Wakefield et al., 2003), 6/19 *FoxO4*$^{-/-}$ females, generally over 2 years of age, developed this neoplasm compared with 0/11 age-matched *FoxO4*$^{+/+}$ (p=0.0613) and 2/15 *FoxO4*$^{-/+}$ (p=0.2569) females. Since FoxOs have been linked to p27^{Kip1} regulation (Medema et al., 2000), we emphasize that these prolactinomas are distinct from the intermediate lobe pituitary adenomas arising in p27^{Kip1} and Rb mutant mice (Fero et al., 1996; Hu et al., 1994; Kiyokawa et al., 1996; Mahler et al., 1996; Nakayama et al., 1996; Wakefield et al., 2003). Consistent with a minor tumor suppressor role for FoxO4, treatment with the carcinogen 7,12-dimethylbenz-alpha-anthracene (DMBA) did not reveal significant differences in median survival (23.4 weeks for *FoxO4*$^{-/-}$ and 27.3 weeks for *FoxO4*$^{+/+}$, p=0.4926) or in tumor incidence or spectrum, although *FoxO4*$^{-/-}$ animals showed a modest increase in lymphoma incidence that approached statistical significance (p=0.053, Fisher Exact Test) (Supplemental Figure S5a and b).

Aged *FoxO3*$^{-/-}$ mice are prone to dermatitis between 10-24 months of age and 15/35 *FoxO3*$^{-/-}$ mice required euthanasia due to progressive skin ulceration (Supplemental Figure S3c and d). The basis of this dermatitis has not been explored. Of the remaining dermatitis-free *FoxO3*$^{-/-}$ mice, 19/20 mice developed tumors (Supplemental Figure S4c and d, p=0.0010; Figures S3e and f). While *FoxO3*$^{-/-}$ females show a more rapid onset of tumors, this relates to increased occurrence of ovarian stromal neoplasms (4/16 *FoxO3*$^{-/-}$ versus 0/10 *FoxO3*$^{+/+}$ females; p=0.1358) and a shorter latency and increased growth of pituitary prolactinomas (7/16 *FoxO3*$^{-/-}$ versus 1/10 *FoxO3*$^{+/+}$ females; p=0.0989) (Supplemental Figures S4e and f, Table S1) which are likely due to elevated gonadotropins associated with premature ovarian failure (Castrillon et al., 2003) and the predisposition of aged FVB/n females to prolactinomas (Mahler et al., 1996; Wakefield et al., 2003). Finally, *FoxO3* status did not alter the outcome of DMBA exposure studies with respect to overall survival and tumor incidence and spectrum (Supplemental Figures S5c and d), with the exception of angiosarcomas, which had an increased incidence in *FoxO3-/+* (p=0.036) and -/- (p=0.364) versus +/+ animals. Thus, *FoxO3* deficiency is associated with a modest tumor phenotype that emerges very late in life and is dominated by neoplasms driven by an abnormal hormonal milieu in females, and a modest increase in the incidence of angiosarcomas but not overall cancer incidence following carcinogen treatment.

To begin to address possible redundancy among FoxO family members, compound germline mutant mice and controls were generated and subjected to detailed long-term phenotypic analyses. *FoxO3*$^{-/-}$ *FoxO4*$^{-/-}$ mice (n=31), followed for up to 100 weeks of age, did not exhibit new phenotypes, change in overall survival, or exacerbation of physiological anomalies beyond those observed in the *FoxO3*$^{-/-}$ mice (e.g., hemolytic anemia, ovarian failure, etc), or increased tumor incidence (Supplemental Figure S6). Lastly, through 80 weeks of observation, *FoxO1*$^{-/+}$ *FoxO3*$^{-/-}$ *FoxO4*$^{-/-}$ mice do not display changes in tumor incidence and spectrum (data not shown). These studies included exhaustive comparisons with *FoxO3*$^{+/+}$ *FoxO4*$^{+/+}$ and

FoxO3$^{-/+}$ *FoxO4*$^{-/-}$ controls (As noted above, the detailed tumor incidence, spectrum, and overall survival data pertaining to these cohorts are presented in Supplemental Figures S3-S6, and Table S1).

Vascular neoplasms in aging *Mx-Cre*$^{+}$ mice of various *FoxO* genotypes. Discrete liver hemangiomas and occasional angiosarcomas were seen in aged *Mx-Cre*$^{+}$*;* *FoxO1*$^{L/L}$ (1 mouse (at 85 weeks) of 5 mice that died at 53-100 weeks and 3 of 4 mice examined at 87-104 weeks of age), *Mx-Cre*$^{+}$*;FoxO1/3*$^{L/L}$ (7 of 10 mice that died at 50-82 weeks and 2 of 2 mice examined at 90-102 weeks) and *Mx-Cre*$^{+}$*;FoxO1/4*$^{L/L}$ mice (5 of 7 mice that died at 58-86 weeks and 2 of 2 mice examined at 96-98 weeks).

Supplemental Methods

Targeting constructs. *FoxO3*$^{-/-}$ mice were generated as described (Castrillon et al., 2003). We cloned and mapped the *FoxO1* and *FoxO4* genomic regions encompassing both coding exons from a bacterial artificial chromosome library. The targeting vector pKOII (courtesy Nabeel Bardeesy) carries a negative selection marker for diphtheria toxin (DT), a positive selection marker for neomycin resistance (Neo), Frt sites (white rectangles) and loxP sites (gray triangles). For *FoxO4*, the first coding exon (containing the start codon and encoding the N-terminal half of the full-length protein) was targeted. For *FoxO1*, the second major coding exon (encoding the C-terminal half of the full-length protein) was targeted. We electroporated TC1 embryonic stem cells and selected transfected cells by standard techniques. We screened 96 clones for each of the three loci using a genomic probe external to the targeting construct (Supplemental Figure S1 and S2) to identify recombinants that contained the Neo selection cassette and both loxP sites. Blastocyst injections were carried out and transmitting chimeric mice were bred with EIIa-Cre transgenic(Lakso et al., 1996) mice to generate the null alleles, and with ACT-FlpE mice (courtesy of Susan Dymecki) to generate the conditional/floxed alleles. Each allele was backcrossed three times to FVB/n females and progeny of these matings that were Cre$^-$ and Flp$^-$ were then intercrossed with littermates to generate the experimental cohorts. Mice were genotyped by multiplex PCR (primers and conditions are available on request).

Generation of mice for aging and tumorigenesis studies. Due to the location of *FoxO4* on the X chromosome, it is not possible to generate *FoxO4*$^{-/+}$ males or littermate *FoxO4*$^{+/+}$ and $^{-/-}$ females. Otherwise, all experimental and control animals were matched littermates. For the Mx-Cre studies, an *Mx-Cre*$^{+}$ male (courtesy of Klaus Rajewsky) was mated with a *FoxO1*$^{L/L}$*; FoxO3*$^{L/L}$*; FoxO4*$^{L/L}$ (*FoxO1/3/4*$^{L/L}$) female, and the progeny were then crossed with *FoxO1/3/4*$^{L/L}$ mice. The resulting offspring were intercrossed to generate mice of the desired genotypes. Litters were treated starting at 4-5 weeks with 3 intraperitoneal injections every other day of 300 µg of polyinosine-polycytidylic acid (pI-pC), a synthetic analog of double-stranded RNA (Invivogen), to induce expression of interferon-beta, thereby leading to transient activation of *Mx-Cre*.

Whole animal and tumor analysis. Littermate controls were analyzed for tumor-free survival. Animals were genotyped by PCR and allowed to age undisturbed in a maximum of 5 mice per cage with standard chow and water *ad libitum* in a standard light-day cycle. Mice were monitored three times a week and were sacrificed when moribund or if external tumors exceeded 2 cm in diameter and scored as a death in survival analysis. Those animals with cancer, as determined by histological analysis, were scored as an event in the tumor-free survival Kaplan−Meier analysis. For lung tumors, analysis of tumor load was carried out as done previously (Zhang et al., 2001).

DMBA treatment. Seven-day old pups were treated with 5% 7,12-dimethylbenz-alpha-anthracene (DMBA) in acetone by pipetting 50µl onto the back, and allowing it to air-dry. Mice were monitored three times a week for signs of morbidity and underwent full autopsies for tumor detection.

Analysis of *Rosa26-lacZ* reporter mice. B6, 129-GtRosa26^{tm1Sor} mice (no. 3309, Jackson Laboratory, Bar Harbor, ME) were used as a reporter strain. Organs were harvested from an *Mx-Cre*$^{+}$*; Rosa26-lacZ*$^{+}$ female and an *Mx-Cre*$^{-}$*; Rosa26-lacZ*$^{+}$ female (both injected with pI-pC) and cut into 1-2 mm pieces. After fixation with 4% paraformaldehyde + 0.25% glutaraldehyde in PBS for 2 hours, tissues were stained for 24 hours in the dark and postfixed in formalin. Tissues were embedded in paraffin and sections were stained with Nuclear Fast Red or left unstained.

Isolation and characterization of endothelial cells (ECs). Livers of *Mx-Cre*$^{+}$ *or Mx-Cre*$^{-}$ mice injected with pI-pC 3 weeks prior were used for the isolation of liver ECs. Liver tissues were homogenized and digested in collagenase D and lysates were run through a cell strainer. ECs were enriched by taking the interphase of a 30% Histodenz (Sigma) and RPMI suspension of cells overlaid after spinning at 1500xg for 20min. Cells were further affinity isolated by CD31-M450 prebound magnetic beads. Isolation of lung ECs and Matrigel morphogenesis assays were carried out as previously described (Balconi et al., 2000) and cells were grown on dishes coated with bovine fibronectin (Sigma). VEGF and basic FGF were obtained from the Biological Resources Branch, NCI Preclinical Repository. Cells were grown in DMEM + 0.5% BSA supplemented with 100 ng/ml VEGF, 100 ng/ml FGF, or 10% FBS. EC proliferation and apoptosis were measured with the BrdU labelling and detection kit (Roche) and the In situ cell death detection kit (Roche), respectively per the manufacturer's instruction. Viability of cells after various treatments was measured by MTT (2,3-bis-(2-methoxy-4-nitro-5-sulfophenyl)-2H-tetrazolium-5-carboxanilide) assays in 96 well plates. Knockdown of mouse Sprouty2 was performed by transfection using FuGENE6 (Roche) of shRNA constructs provided by Dr. William Hahn, Dana Farber Cancer Institute. The shRNA constructs shSpry2_1 and _2 correspond to clone ID#s TRCN0000007521 and 7523, respectively (The DFCI-Broad RNAi Consortium, commercially available from Sigma-Aldrich). Vector (pLKO) alone and pLKO-GFP were used as controls to exclude non-specific responses. Cells were selected for 96 hrs with puromycin (1µg/ml) and used for further assays. Additional shRNAs used are listed below.

Microarray analysis. Freshly isolated lung ECs and liver ECs were grown on fibronectin-coated plates for 72 hours. RNA was isolated using Trizol (Invitrogen) and the RNeasy mini kit (Qiagen). Gene expression profiling was performed utilizing the Affymetrix 430 2.0 chips. dChip (Li and Wong, 2001; Li and Wong, 2003) was used to normalize arrays and to compute expression indices. The log transformed expression indices x_{ijk} (*i*-gene, *j*-condition, *k*-replicate) were modeled using a hierarchical empirical Bayes model which assumes (i) $x_{ijk} \mid \mu_{ij}, \sigma_i^2 \sim N(\mu_{ij}, \sigma_i^2)$; (ii) $\mu_{ij} \mid \mu_0, \tau_0^2 \propto 1$; and (iii) $\sigma_i^2 \mid v_0, \omega_0^2 \sim Inv-\chi^2(v_0, \omega_0^2)$. To select genes, we first estimated the posterior mean of σ_i^2 for each gene using a variance shrinkage estimator (Ji and Wong, 2005), σ_i^2 was then set to its estimate $\hat{\sigma}_i^2$ and fixed. For comparisons between two conditions (e.g., Mx-Cre$^+$ Lung vs. Mx-Cre$^-$ Lung), $t_i = (\bar{x}_{i1} - \bar{x}_{i2}) / (\hat{\sigma}_i \sqrt{1/K_1 + 1/K_2})$ (K_j - the number of arrays within condition *j*) were used to rank genes. For comparisons among three or more conditions (e.g., "[Mx-Cre$^+$ liver EC > Mx-Cre$^-$ liver EC] and [Mx-Cre$^+$ Lung > Mx-Cre$^-$ Lung]"), random samples μ_{ij} were drawn from $N(\bar{x}_{ij}, \hat{\sigma}_i^2 / K_j)$. The empirical frequencies that the pre-specified criterion was satisfied among 1000 Monte Carlo draws were then used to rank genes, and for each gene, one minus the empirical frequency was reported as its score.

FoxO DNA Binding Element Studies. Differentially expressed genes with RefSeq annotations were analyzed for the presence of FoxO BE. The March 2005 version of mouse genome (NCBI build 34) was used in the analysis. A 3rd order Markov chain was used to model the random background sequence. The FoxO matrix was used to scan the target regions. At each position, its likelihood was compared with the likelihood of the background model. A site was picked as a potential FoxO binding site if the likelihood ratio between the FoxO and background model is greater than 250. Potential FoxO binding sites were filtered further by cross-species conservation using two independent approaches. In the first approach (Method1), a conservation score was computed for each position in the genome. FoxO sites whose mean conservation score was among the top 10% of the genome-wide scores were preserved as the conserved FoxO binding sites. To compute the conservation score, multiple alignments between mouse and 9 vertebrate genomes were downloaded from UCSC genome browser (http://genomes.ucsc.edu). A 50bp sliding window was used to scan the alignment. For each window, we counted matched base pairs between species i and j (denoted by I_{ij} , i = mouse; j = human, rat, dog, cow, or zebrafish), and the total number of columns in the pairwise alignment (denoted by N_{ij}). We computed percent identities $\hat{\theta}_{ij} = I_{ij} / N_{ij}$, and derived corresponding z-scores $z_{ij} = (\hat{\theta}_{ij} - \theta_{ij}) \big/ \sqrt{\theta_{ij}(1-\theta_{ij})/N_{ij}}$, where θ_{ij} was the percent identity between species i and j in a 1Mbp surrounding window. The z-scores from five pairwise comparisons (mouse-human, mouse-dog, mouse-cow mouse-chicken, and mouse-zebrafish) were then averaged and converted into the interval [0, 255] to serve as the final conservation score. The higher the score, the more conserved a position was. For each gene, the total number of conserved FoxO sites was shown in Tables 1 and 2, and Log_{10} (likelihood ratio between the FoxO matrix model and background Markov model) of all conserved FoxO sites were added up and the sum shown.

In the second approach (Method2), we selected ortholog genes from human, dog, cow, chicken, and zebrafish for each mouse gene in the gene list. MLAGAN (Brudno et al., 2003) was used to construct the cross-species alignment of target regions. The FoxO matrix was used to scan each species to get potential FoxO binding sites. If a position in the alignment was identified as FoxO binding site in mouse, human and at least one additional species, it was identified as a 3-species conserved FoxO site.

Chromatin Immunoprecipitation (ChIP) assay. Two million liver ECs were crosslinked by addition of 1% formaldehyde to the medium for 10 min followed by quenching with 125mM glycine. The cells were resuspended in lysis buffer (1% SDS, 10 mM EDTA, and 50 mM Tris (pH 8.1), Protease Inhibitor Cocktail II (Roche)), sonicated 10 times for 30 s with 2 min idle time, the lysates were cleared by centrifugation. One hundred microliters of the sheared DNA was diluted 10-fold in dilution buffer (0.01% SDS, 1.1% Triton X-100, 1.2 mM EDTA, 16.7 mM Tris-HCl (pH 8.1), and 167 mM NaCl). Chromatin solution was precleared for 1 h at 4°C with 60 µl of protein G-agarose/salmon sperm DNA. Ten microliters of the precleared chromatin solutions was saved for assessment of input chromatin, and the rest of the precleared chromatin solutions was incubated with 1ug of anti-RNA polymerase II (clone CTD4H8, Upstate) or mixture of anti-FoxO Ab [Afx (FoxO4), FKHR (FoxO1), Cell signalling, FKHRL1(FoxO3), Upstate) overnight at 4°C. Immune complexes were collected on 60 µl of protein A/G Plus-agarose/salmon sperm beads. Precipitates were washed sequentially for 5 min each in Low salt wash buffer [0.1% SDS, 1% Triton X-100, 2 mM EDTA, 20 mM Tris-HCl (pH 8.1), 150 mM NaCl], High salt wash buffer [0.1% SDS, 1% Triton X-100, 2 mM EDTA, 20 mM Tris-HCl (pH 8.1), 500 mM NaCl], LiCl immune wash buffer (Upstate). Precipitates were then washed twice with 1X TE (pH. 8.0) and extracted two times with 1% SDS, 0.1 M $NaHCO_3$. Elutes were incubated at 65°C with 0.25 M NaCl overnight to reverse cross-linking followed by another 1 hr incubation at 45°C with 10 µM EDTA, 40 µM Tris-HCl (pH 6.8) and 2µg Proteinase K (Sigma). The DNA was purified using a PCR purification kit (Qiagen) with 40 µl of distilled water. Two microliters of immunoprecipitated DNA was used for real time

PCR analysis in 25-µl total reaction volumes, and the following primers were used in the ChIP assays:

Primers	forward	reverse
spry_a	catttgtgtgttttggggagagat	cggcagttgggttggaatta
spry_b	tagggcgactcagtggctatc	gaccggagtcaaaggaccttc
spry_c	aattagcaaatggctcccgg	tttgtgactgtgccatgaagc
spry_d	ttccagtcctccaagcaatctag	agtgcctccaggaagggaat

primers	forward	reverse
ADM_a	tttgttgctgtcaaggttttt	cgctctccaccttacacaca
ADM_b	gattggagggttcgtcttga	aaaactcagctgcctgtgtg
CITED_c	taattgtccttgcggagctt	ggagcactcaccttggtttt
CITED_d	ggtcgctttaggcagagaaa	ggaagcaagaccacagaagg
CITED_e	ttgcagtggactggcttaaa	taggtgggtctcatgtgctg
CTGF_f	acgagcctgcaagctatttg	acgatgttgttggggtttgt
CCRN4L_g	ggcttgtgagcattgtgaaa	gaggggaagtaccagtgttca
CCRN4L_h	tttcaagaaaggaaaccgaaaa	agtgcgcttttgtttgtttg
BMPER_I	aggcatctagccatggtgtt	gcttagcatgctccatttcc
BMPER_j	ttttcaggcaggtgaagacc	tgaagcgcaatctctttcct
MRC1_k	tgttcctctctccccttcct	ggagctgcctgactgaaaag
PBX1_l	agccttcatgggcttttgat	ggttaccaagggtggtgcta
PBX1_m	ctcacgggtgtctttgacct	ttgttagggggtcctgtttg

PCR conditions were as follows: 30 cycles of 94°C for 30s, 55°C for 30s, and 72°C for 30s. Twenty microliters of PCR products were analyzed by 2% TBE agarose gel containing ethidium bromide.

RNA *in situ* hybridization (RISH). Tissues were fixed in 4% paraformaldehyde overnight, frozen in OCT and cryosectioned (10 micron-thick sections). ISH was performed as previously described (Gray et al. 2004). Full length cDNA was used to generate probes. FoxO1, 3, and 4 cDNAs were PCR cloned into pCRII vector and in vitro transcribed. TCF4, KLF6, MEIS1, and PBX1 cDNAs were generously provided by Dr. Qiufu Ma; the remaining cDNAs were purchased from a commercial source (Open Biosystems).

ShRNAs used for knockdown studies. All the shRNAs were acquired through TRC. Clone and source ID are as below.

sourceId	symbol	cloneId	cloneName
18514	Pbx1	TRCN0000012573	NM_008783.1-2445s1c1
18514	Pbx1	TRCN0000012574	NM_008783.1-1478s1c1
18514	Pbx1	TRCN0000012577	NM_008783.1-1036s1c1
12443	Ccnd1	TRCN0000026883	NM_007631.1-608s1c1
12443	Ccnd1	TRCN0000026951	NM_007631.1-254s1c1
12443	Ccnd1	TRCN0000026948	NM_007631.1-706s1c1
12443	Ccnd1	TRCN0000026881	NM_007631.1-511s1c1
12443	Ccnd1	TRCN0000026910	NM_007631.1-879s1c1
17533	Mrc1	TRCN0000054795	NM_008625.1-4070s1c1
17533	Mrc1	TRCN0000054796	NM_008625.1-1351s1c1
17533	Mrc1	TRCN0000054797	NM_008625.1-2687s1c1
15901	Id1	TRCN0000071433	NM_010495.1-331s1c1
15901	Id1	TRCN0000071435	NM_010495.1-476s1c1
15901	Id1	TRCN0000071437	NM_010495.1-103s1c1
21807	TSC22D	TRCN0000086178	NM_009366.1-251s1c1
21807	TSC22D	TRCN0000086179	NM_009366.1-418s1c1
21807	TSC22D	TRCN0000086180	NM_009366.1-290s1c1
21807	TSC22D	TRCN0000086181	NM_009366.1-227s1c1
21807	TSC22D	TRCN0000086182	NM_009366.1-409s1c1
11535	Adm	TRCN0000098030	NM_009627.1-979s1c1
11535	Adm	TRCN0000098031	NM_009627.1-259s1c1
11535	Adm	TRCN0000098032	NM_009627.1-434s1c1
11535	Adm	TRCN0000098034	NM_009627.1-530s1c1
73230	Bmper	TRCN0000114776	NM_028472.1-3282s1c1
73230	Bmper	TRCN0000114777	NM_028472.1-2525s1c1
73230	Bmper	TRCN0000114778	NM_028472.1-867s1c1
73230	Bmper	TRCN0000114779	NM_028472.1-1105s1c1
73230	Bmper	TRCN0000114780	NM_028472.1-2277s1c1
12457	Ccrn4l	TRCN0000099675	NM_009834.1-2115s1c1
12457	Ccrn4l	TRCN0000099676	NM_009834.1-1389s1c1
12457	Ccrn4l	TRCN0000099677	NM_009834.1-1636s1c1
12457	Ccrn4l	TRCN0000099678	NM_009834.1-1642s1c1
12457	Ccrn4l	TRCN0000099679	NM_009834.1-1333s1c1
14219	Ctgf	TRCN0000109665	NM_010217.1-2079s1c1
14219	Ctgf	TRCN0000109666	NM_010217.1-572s1c1
14219	Ctgf	TRCN0000109667	NM_010217.1-1239s1c1
14219	Ctgf	TRCN0000109668	NM_010217.1-789s1c1
14219	Ctgf	TRCN0000109669	NM_010217.1-1041s1c1

Supplemental Figure Legends

Supplemental Figure S1: Generation of *FoxO1* conditional and null alleles. a, Schematic of *FoxO1* targeting vector. LoxP sites were inserted into intronic sites flanking the second exon of *FoxO1*. PCR primers are indicated with arrows. **b**, Southern analysis of DNA from ES clones to demonstrate recombination. DNA was digested with HindIII+ SspI (left panel) and SpeI (right panel). **c**, PCR genotyping of wild type, floxed, and null alleles using primers a + b + d. **d**, Confirmation of *FoxO1* deletion and loss of expression in *FoxO1* null MEFs by Northern analysis.

Supplemental Figure S2: Generation of *FoxO4* conditional and null alleles. a, Schematic of *FoxO4* targeting vector. LoxP sites were inserted into intronic sites flanking the first exon of *FoxO4*. PCR primers are indicated with arrows. **b**, Southern analysis of DNA from ES clones to demonstrate recombination. DNA was digested with XhoI + NcoI. **c**, PCR genotyping of wild type, floxed, and null alleles using primers d + e + m. **d**, Confirmation of *FoxO4* deletion and loss of expression in *FoxO4*$^{-/-}$ skeletal muscle by Northern analysis.

Supplemental Figure S3: Analysis of FoxO germline knockouts. a, Overall survival of *FoxO1*$^{-/+}$ mice. **b**, Overall survival of *FoxO4*$^{-/-}$ mice. **c**, Overall survival of *FoxO3*$^{-/-}$ mice. **d**, Overall survival of *FoxO3*$^{-/-}$ mice with dermatitis. For d-f, *FoxO3*$^{-/-}$ mice are divided into two groups: those sacrificed due to dermatitis, and those without dermatitis-associated morbidity. **e**, Tumor-free survival of *FoxO3*$^{-/-}$ males. **f**, Tumor-free survival of *FoxO3*$^{-/-}$ females. **g**, Lung tumor load (total tumor volume) in *FoxO4*$^{+/+}$ (n=8) and *FoxO4-/-* (n=15) mice. **h**, Histology of *FoxO4*$^{-/-}$ lung tumors, hematoxylin and eosin stains. Scale bars: 500 µm (low magnification) and 100 µm (high power).

Supplemental Figure S4: Tumor-free survival of single and compound (germline) *FoxO* mutant mice. a, *FoxO1*. **b**, *FoxO4*. **c**, *FoxO3*. **d**, *FoxO3* with exclusion of dermatitis-associated deaths. **e**, Pituitary adenomas in *FoxO3* females. Left to right: normal pituitary (*FoxO3*$^{+/+}$), small pituitary adenoma (*FoxO3*$^{+/+}$), and large pituitary adenoma (*FoxO3*$^{-/-}$). Black dashed lines demarcate pituitary gland; white dashed lines demarcate pituitary adenomas. **f,** Pituitary tumor histology, hematoxylin and eosin stain. Adenoma shows monomorphic cell population. Scale bar: 100 µm.

Supplemental Figure S5: Analysis of DMBA-treated FoxO germline knockouts. a, Survival of DMBA-treated *FoxO4*$^{-/-}$ mice. Pups were treated with DMBA at day 7. Mice underwent full autopsies and histopathologic analysis. **b**, Tumor development in DMBA-treated *FoxO4*$^{-/-}$ mice. Total numbers of each genotype are indicated. For the incidence of angiosarcomas in the uterus, percentages were calculated from total number of females only. **c**, Survival of DMBA-treated *FoxO3*$^{-/-}$ mice. **d**, Tumor development in DMBA-treated *FoxO3*$^{-/-}$ mice.

Supplemental Figure S6: Analysis of compound *FoxO3*/*FoxO4* germline knockouts. a, Overall survival of *FoxO4*$^{-/-}$*; FoxO3*$^{-/-}$ and *FoxO4*$^{-/-}$*; FoxO3*$^{-/+}$ littermates and *FoxO4*$^{+/+}$*; FoxO3*$^{+/+}$ control mice. Survival of *FoxO3*$^{-/-}$ mice is plotted for comparison. **b**, Tumor-free survival of compound *FoxO4*$^{-/-}$*; FoxO3*$^{-/-}$ mice. **c**, Tumor spectra of mice with compound germline *FoxO* mutations. *FoxO4*$^{-/-}$*; FoxO3*$^{-/-}$ mice (n=31) were analyzed in relation to *FoxO4*$^{-/-}$*; FoxO3*$^{-/+}$ (n=26) littermates and *FoxO4*$^{+/+}$*; FoxO3*$^{+/+}$ mice (n=28).

Supplemental Figure S7: Abnormal vascular lesions in *Mx-Cre*$^{+}$ mice and intermediate controls. a-d, hematoxylin and eosin-stained tissue sections. **a**, *Mx-Cre*$^{+}$ mice (20-43 weeks). i, adrenal gland (medulla replaced by hemorrhage, *=region of hemorrhage; scale bar=400 µm), ii, Hemangiomatous change in liver (scale bar=200 µm), iii, bone marrow (left: bone marrow from *Mx-Cre*$^{-}$ mouse; right: bone marrow from *Mx-Cre*$^{+}$ mouse; scale bar=100 µm), iv, skin (scale bar=200 µm), v, perirenal fat hemangioma, (scale bar=200 µm), vi, hemorrhagic lymph node (scale bar=500 µm). **b**, Uterine horn from 60-week *Mx-Cre*$^{+}$*;FoxO1*$^{L/L}$. i, low power (scale bar=2 mm), ii, high power of boxed region from (i) (scale bar=500 µm). **c**, Uterine horn and perirenal fat hemangioma from 60-week *Mx-Cre*$^{+}$*;FoxO1/4*$^{L/L}$ mouse. i, uterine horn, low power (scale bar=2 mm); ii, uterine horn, high power (scale bar=500 µm); iii, perirenal fat hemangioma (scale bar=200 µm). **d**, *Mx-Cre*$^{+}$*;FoxO1/3*$^{L/L}$ mouse (50 weeks). Depicted are: uterine horn (low (i) and high (ii) power), adipose tissue (iii), and skin (iv). Scale bars: 500 µm, (i), 50 µm (ii), 200 µm (iii and iv).

Supplemental Figure S8. *Mx-Cre* transgene results in broad Cre-mediated recombination in endothelium and most epithelia following pI-pC treatment.

a, *Rosa26-lacZ* reporter mice 6 months after pI-pC treatment. a, Liver (inset=control liver). b, Thymus. c, Lung. Liver, thymus, and lung parenchymal cells show very high levels of recombination. d, Pancreas. e, Salivary gland (submandibular). Both pancreas and salivary gland showed high levels of recombination in ductal epithelium, and a low frequency of recombination in acinar cells. f, Mammary gland with essentially complete recombination. g, Skin. h, Small intestine. Skin and small intestine epithelial cells exhibited subtotal recombination; distinct clones of positive cells were observed. i, Renal tubules. j, Brain. k, Abdominal muscle. Brain and skeletal muscle exhibited a very low frequency of recombination, except for endothelial cells where recombination frequencies approached 100%, as was the case in other tissues. The blue staining surrounding myofibers corresponds to capillary endothelium. l, uterus with high frequency of recombination in endothelial cells and in some myometrial cells, particularly those of the outer layer (bottom edge of figure). Scale bar = 120 µm (d, e); 60 µm (a, f, g, h, i, k); 40 µm (b, c, j, l). **b,** Quantitative real-time PCR analysis of FoxO deletion in *Mx-Cre*$^{+}$ mice. Tissues were harvested from 2-3 sets each of *Mx-Cre*$^{+}$ and *Mx-Cre*$^{-}$mice and RNA was isolated and analyzed for *FoxO1*, *FoxO3*, or *FoxO4* expression.

Supplemental Figure S9. Characterization of isolated ECs. At 96hr post isolation both lung and liver EC are CD31+ above 97% by flowcytometry analysis (a) and immunofluorescence for CD31 and VE-cadherin shown in red (b). **b.** right panels, mixed cells from a mouse lung were used as specificity controls (blue, DAPI). Arrows indicate lung EC stained positive for CD31 or VE-cadherin within the same microscopic field with non-EC. **c**. comparable deletions of FoxO1,3,4 in both lung and liver EC were examined by immunoblotting (c) and PCR analysis (d). Note comparable expression of FoxO in liver and lung EC. FoxO4 protein is normally detected by FoxO1 antibody and is under the detection limit in EC.

Supplemental Figure S10. *In situ* hybridization for FoxO1/3/4. 3 weeks after pI-pC injection lung, uterus, and liver tissues were harvested from *Mx-Cre*$^{-}$ and *Mx-Cre*$^{+}$*;FoxO1/3/4*$^{L/L}$ mouse and examined for FoxO mRNA expression by RISH.

Supplemental Figure S11. In situ hybridization for FoxO target genes. RISH was performed for predicted FoxO targets genes as in Supplemental Figure S10. Note differential expression of indicated genes in the vascular endothelium.

Supplemental Figure S12. ChIP analysis for FoxO target genes. FoxO BE conserved in more than 3 species was tested for FoxO binding by ChIP analysis. Summary of FoxO BE coordinates and results are presented in the table (left). Indicated PCR products from 25-35 cycles were run on 1.5% agarose gel with EtBr and inverted images were taken with imager.

Supplemental Figure S13. Effect on EC viability by knockdown of other FoxO target genes. Expression of randomly chosen FoxO target genes was suppressed by combined shRNAs for each gene in pLKO-lentiviral vectors. Efficiency of knockdown was measured by RT-qPCR (a). Note genes upregulated in *Mx-Cre*$^{+}$ liver EC were knocked down to 30~40% and expression of those downregulated were knocked down to 40~50% level in *Mx-Cre*$^{-}$ liver EC in order to simulate their FoxO-dependent expression pattern. Effect of knockdown on EC viability was measured by BrdU incorporation (b) and TUNEL assay (c). *, $p<0.05$.

Supplemental Tables

Supplemental Table S1. Tumor spectra of mice with germline mutation of a single *FoxO* gene. For pituitary adenomas and female-specific tumors, mice are separated by gender for analysis of incidence.

Supplemental Table S2. List of top 600 differentially expressed genes (~300 up or down) from *Mx-Cre*$^{+}$ and *Mx-Cre*$^{-}$ thymocytes. 354 most differentially regulated genes used for FoxO BE study were highlighted.

Supplemental Table S3. List of top 600 genes (~300 up or down) showing greater fold changes in liver EC from *Mx-Cre*$^{+}$ and *Mx-Cre*$^{-}$ compared to no significant changes in lung EC. 138 most differentially regulated genes used for FoxO BE study were highlighted.

References

Balconi, G., Spagnuolo, R., and Dejana, E. (2000). Development of endothelial cell lines from embryonic stem cells: A tool for studying genetically manipulated endothelial cells in vitro. Arterioscler Thromb Vasc Biol *20*, 1443-1451.
Brudno, M., Do, C.B., Cooper, G.M., Kim, M.F., Davydov, E., Green, E.D., Sidow, A., and Batzoglou, S. (2003). LAGAN and Multi-LAGAN: efficient tools for large-scale multiple alignment of genomic DNA. Genome Res *13*, 721-731.
Castrillon, D.H., Miao, L., Kollipara, R., Horner, J.W., and DePinho, R.A. (2003). Suppression of ovarian follicle activation in mice by the transcription factor Foxo3a. Science *301*, 215-218.
Fero, M.L., Rivkin, M., Tasch, M., Porter, P., Carow, C.E., Firpo, E., Polyak, K., Tsai, L.H., Broudy, V., Perlmutter, R.M.*, et al.* (1996). A syndrome of multiorgan hyperplasia with features of gigantism, tumorigenesis, and female sterility in p27(Kip1)-deficient mice. Cell *85*, 733-744.
Furuyama, T., Kitayama, K., Shimoda, Y., Ogawa, M., Sone, K., Yoshida-Araki, K., Hisatsune, H., Nishikawa, S., Nakayama, K., Ikeda, K.*, et al.* (2004). Abnormal angiogenesis in Foxo1 (Fkhr)-deficient mice. The Journal of biological chemistry *279*, 34741-34749.
Hosaka, T., Biggs, W.H., 3rd, Tieu, D., Boyer, A.D., Varki, N.M., Cavenee, W.K., and Arden, K.C. (2004). Disruption of forkhead transcription factor (FOXO) family members in mice reveals their functional diversification. Proc Natl Acad Sci U S A *101*, 2975-2980.
Hu, N., Gutsmann, A., Herbert, D.C., Bradley, A., Lee, W.H., and Lee, E.Y. (1994). Heterozygous Rb-1 delta 20/+mice are predisposed to tumors of the pituitary gland with a nearly complete penetrance. Oncogene *9*, 1021-1027.
Ji, H., and Wong, W.H. (2005). TileMap: create chromosomal map of tiling array hybridizations. Bioinformatics *21*, 3629-3636.
Kiyokawa, H., Kineman, R.D., Manova-Todorova, K.O., Soares, V.C., Hoffman, E.S., Ono, M., Khanam, D., Hayday, A.C., Frohman, L.A., and Koff, A. (1996). Enhanced growth of mice lacking the cyclin-dependent kinase inhibitor function of p27(Kip1). Cell *85*, 721-732.
Kuhn, R., Schwenk, F., Aguet, M., and Rajewsky, K. (1995). Inducible gene targeting in mice. Science *269*, 1427-1429.
Lakso, M., Pichel, J.G., Gorman, J.R., Sauer, B., Okamoto, Y., Lee, E., Alt, F.W., and Westphal, H. (1996). Efficient in vivo manipulation of mouse genomic sequences at the zygote stage. Proc Natl Acad Sci U S A *93*, 5860-5865.
Li, C., and Wong, W.H. (2001). Model-based analysis of oligonucleotide arrays: expression index computation and outlier detection. Proc Natl Acad Sci U S A *98*, 31-36.
Li, C., and Wong, W.H. (2003). DNA-Chip Analyzer (dChip). In The analysis of gene expression data: methods and software, G. Parmigiani, G. E.S., R. Irizarry, and S.L. Zeger, eds. (Springer).
Mahler, J.F., Stokes, W., Mann, P.C., Takaoka, M., and Maronpot, R.R. (1996). Spontaneous lesions in aging FVB/N mice. Toxicol Pathol *24*, 710-716.
Medema, R.H., Kops, G.J., Bos, J.L., and Burgering, B.M. (2000). AFX-like Forkhead transcription factors mediate cell-cycle regulation by Ras and PKB through p27kip1. Nature *404*, 782-787.

Nakayama, K., Ishida, N., Shirane, M., Inomata, A., Inoue, T., Shishido, N., Horii, I., and Loh, D.Y. (1996). Mice lacking p27(Kip1) display increased body size, multiple organ hyperplasia, retinal dysplasia, and pituitary tumors. Cell *85*, 707-720.
Wakefield, L.M., Thordarson, G., Nieto, A.I., Shyamala, G., Galvez, J.J., Anver, M.R., and Cardiff, R.D. (2003). Spontaneous pituitary abnormalities and mammary hyperplasia in FVB/NCr mice: implications for mouse modeling. Comp Med *53*, 424-432.
Zhang, Z., Wang, Y., Vikis, H.G., Johnson, L., Liu, G., Li, J., Anderson, M.W., Sills, R.C., Hong, H.L., Devereux, T.R.*, et al.* (2001). Wildtype Kras2 can inhibit lung carcinogenesis in mice. Nat Genet *29*, 25-33.

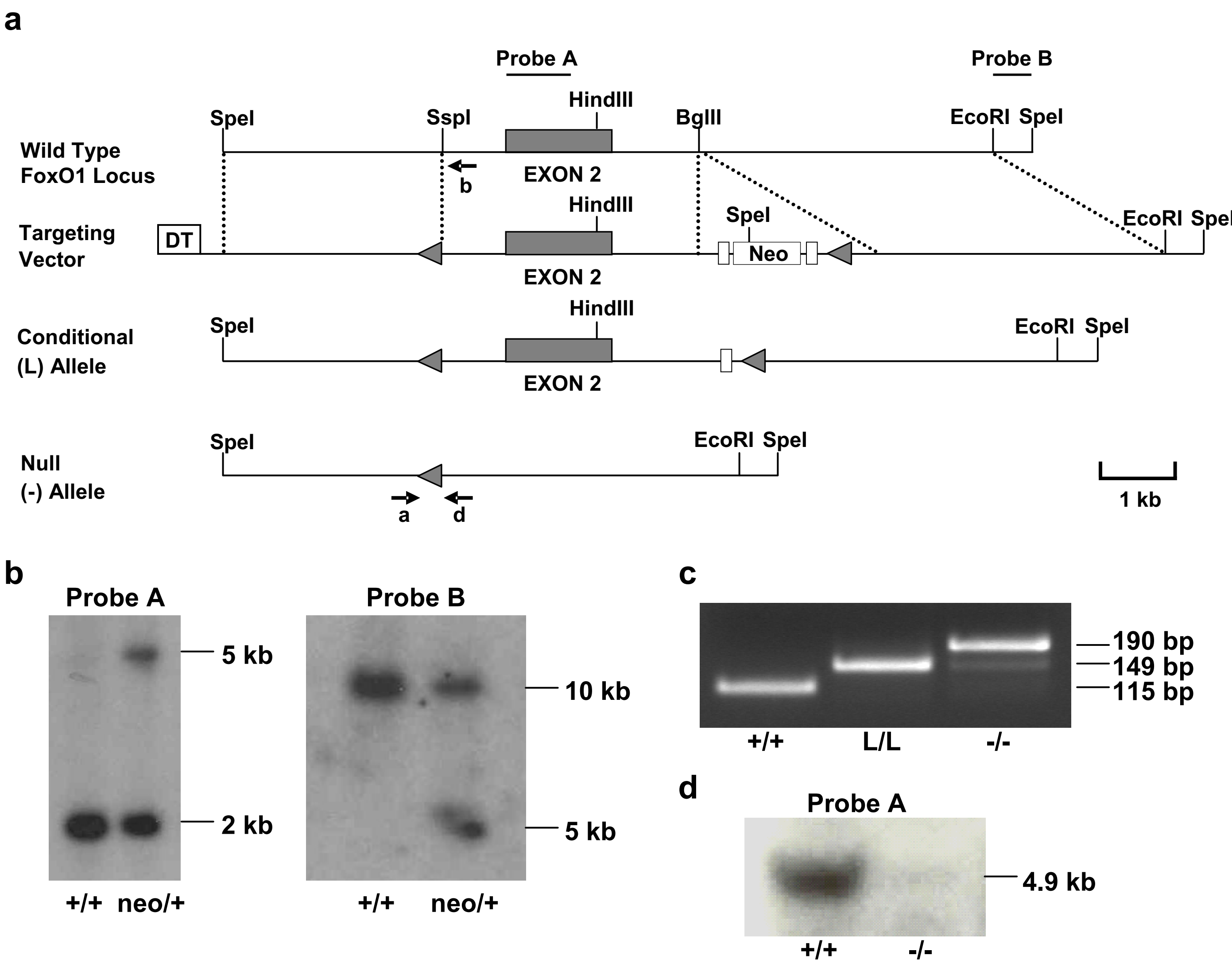
a
Probe A
Probe B
HindIII
SpeI
SspI
BglII
EcoRI SpeI
Wild Type
FoxO1 Locus
b
EXON 2
HindIII
SpeI
EcoRI SpeI
Targeting
Vector
DT
Neo
EXON 2
HindIII
SpeI
EcoRI SpeI
Conditional
(L) Allele
EXON 2
SpeI
EcoRI SpeI
Null
(-) Allele
a
d
1 kb
b
Probe A
5 kb
2 kb
+/+ neo/+
Probe B
10 kb
5 kb
+/+ neo/+
c
190 bp
149 bp
115 bp
+/+ L/L -/-
d
Probe A
4.9 kb
+/+ -/-

Figure S1.

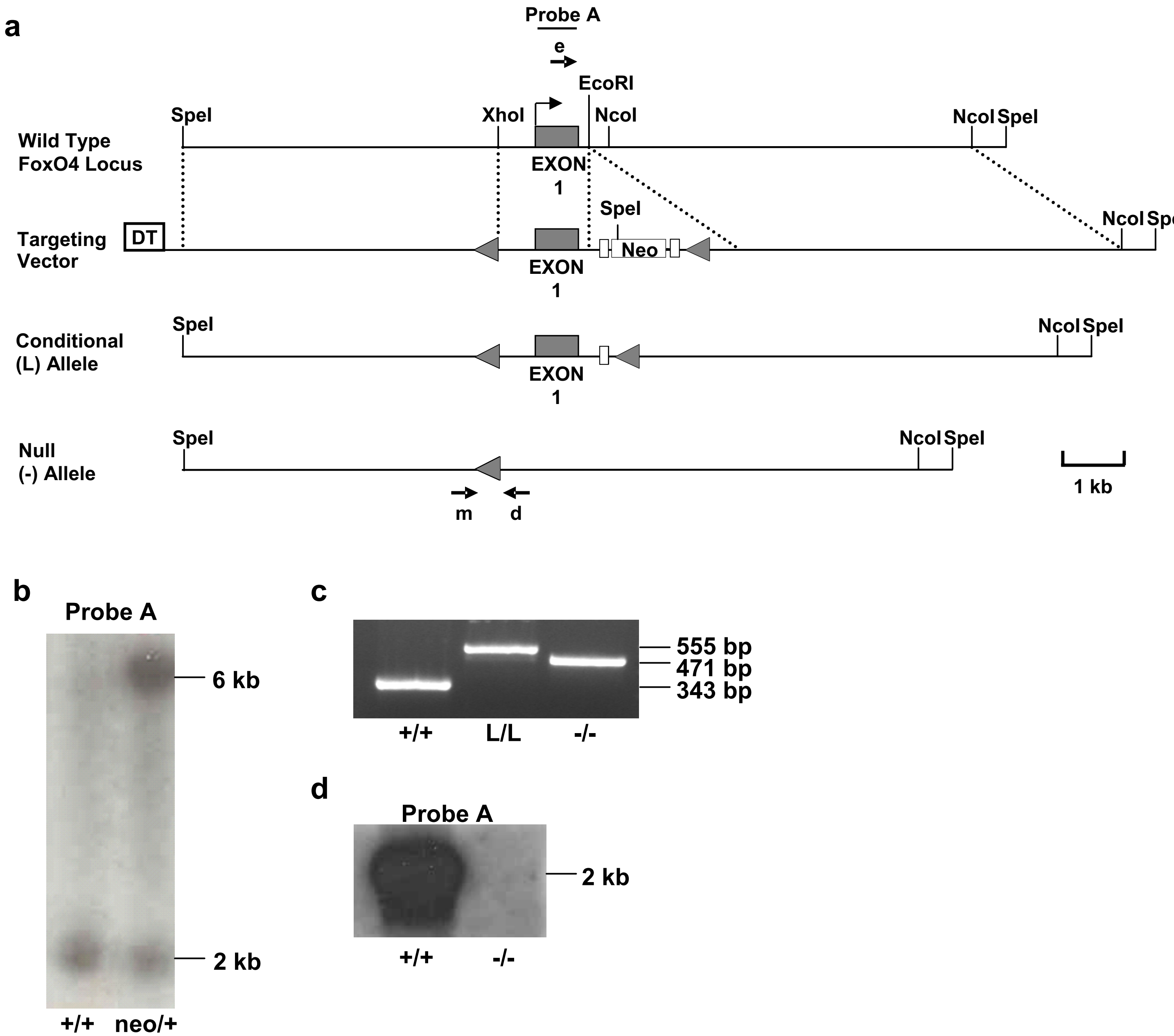
a
Probe A
e
EcoRI
SpeI
XhoI
NcoI
NcoI SpeI
Wild Type
FoxO4 Locus
EXON
1
Targeting
Vector
DT
SpeI
Neo
NcoI SpeI
EXON
1
Conditional
(L) Allele
SpeI
NcoI SpeI
EXON
1
Null
(-) Allele
SpeI
NcoI SpeI
m
d
1 kb
b
Probe A
6 kb
2 kb
+/+
neo/+
c
555 bp
471 bp
343 bp
+/+
L/L
-/-
d
Probe A
2 kb
+/+
-/-

Figure S2.

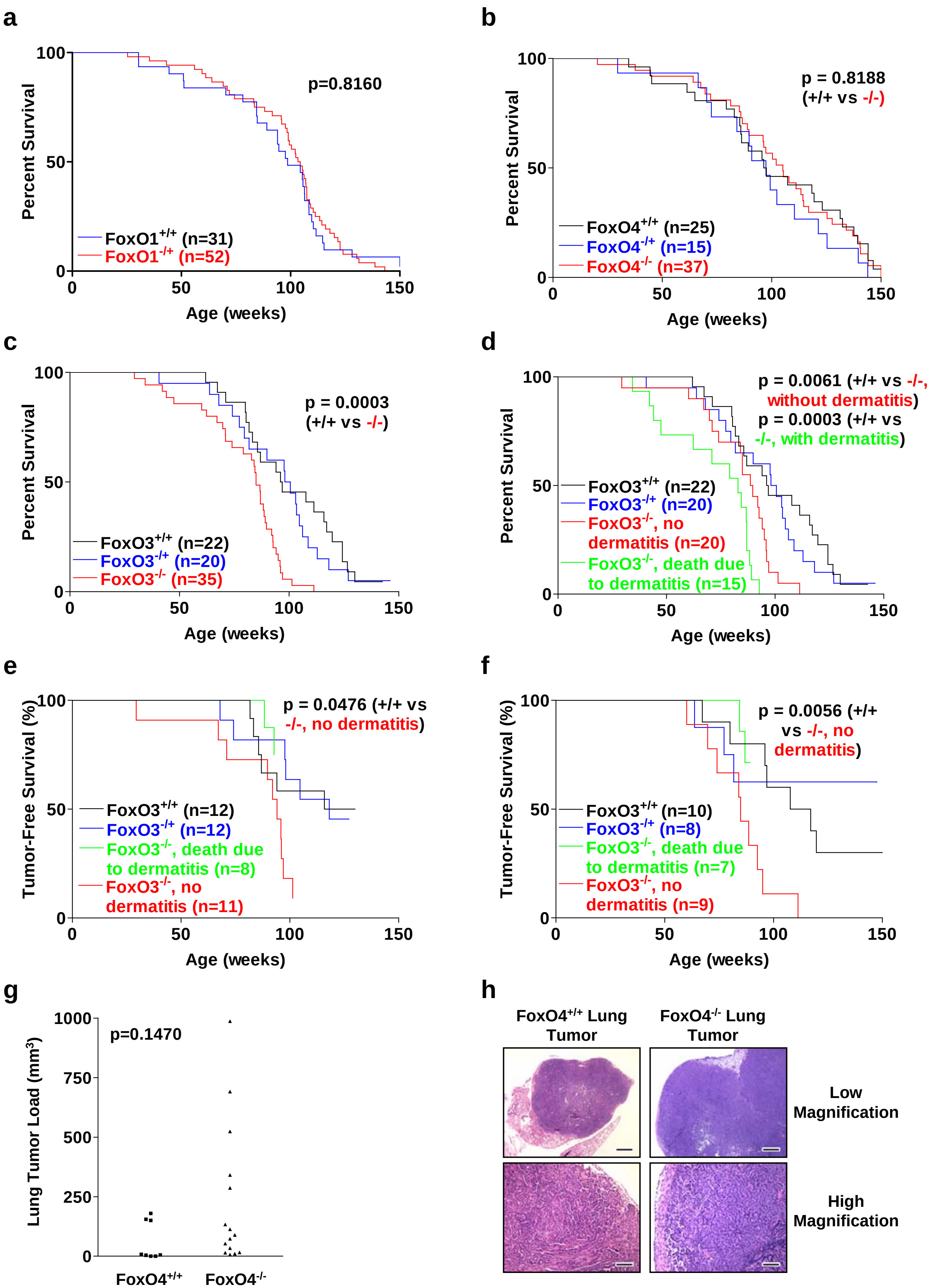
a
Percent Survival
100
50
0
Age (weeks)
p=0.8160
FoxO1+/+ (n=31)
FoxO1-/+ (n=52)
b
Percent Survival
Age (weeks)
p = 0.8188
(+/+ vs -/-)
FoxO4+/+ (n=25)
FoxO4-/+ (n=15)
FoxO4-/- (n=37)
c
Percent Survival
Age (weeks)
p = 0.0003
(+/+ vs -/-)
FoxO3+/+ (n=22)
FoxO3-/+ (n=20)
FoxO3-/- (n=35)
d
Percent Survival
Age (weeks)
p = 0.0061 (+/+ vs -/-,
without dermatitis)
p = 0.0003 (+/+ vs
-/-, with dermatitis)
FoxO3+/+ (n=22)
FoxO3-/+ (n=20)
FoxO3-/-, no
dermatitis (n=20)
FoxO3-/-, death due
to dermatitis (n=15)
e
Tumor-Free Survival (%)
Age (weeks)
p = 0.0476 (+/+ vs
-/-, no dermatitis)
FoxO3+/+ (n=12)
FoxO3-/+ (n=12)
FoxO3-/-, death due
to dermatitis (n=8)
FoxO3-/-, no
dermatitis (n=11)
f
Tumor-Free Survival (%)
Age (weeks)
p = 0.0056 (+/+
vs -/-, no
dermatitis)
FoxO3+/+ (n=10)
FoxO3-/+ (n=8)
FoxO3-/-, death due
to dermatitis (n=7)
FoxO3-/-, no
dermatitis (n=9)
g
Lung Tumor Load (mm3)
1000
750
500
250
0
p=0.1470
FoxO4+/+
FoxO4-/-
h
FoxO4+/+ Lung
Tumor
FoxO4-/- Lung
Tumor
Low
Magnification
High
Magnification

Figure S3.

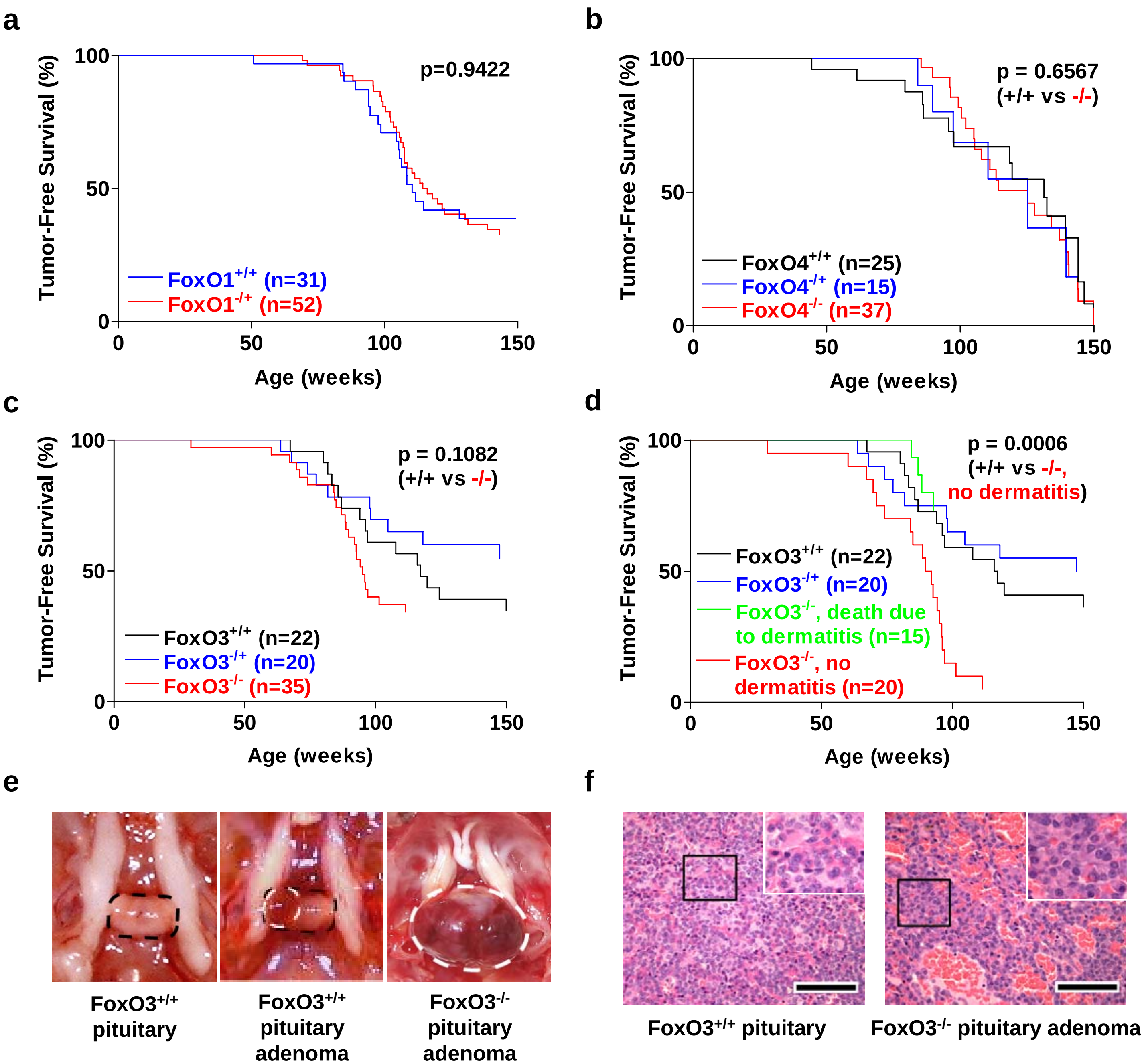

a
Tumor-Free Survival (%)
p=0.9422
FoxO1+/+ (n=31)
FoxO1-/+ (n=52)
Age (weeks)
b
p = 0.6567
(+/+ vs -/-)
FoxO4+/+ (n=25)
FoxO4-/+ (n=15)
FoxO4-/- (n=37)
c
p = 0.1082
(+/+ vs -/-)
FoxO3+/+ (n=22)
FoxO3-/+ (n=20)
FoxO3-/- (n=35)
d
p = 0.0006
(+/+ vs -/-,
no dermatitis)
FoxO3+/+ (n=22)
FoxO3-/+ (n=20)
FoxO3-/-, death due
to dermatitis (n=15)
FoxO3-/-, no
dermatitis (n=20)
e
FoxO3+/+
pituitary
FoxO3+/+
pituitary
adenoma
FoxO3-/-
pituitary
adenoma
f
FoxO3+/+ pituitary
FoxO3-/- pituitary adenoma

Figure S4.

a

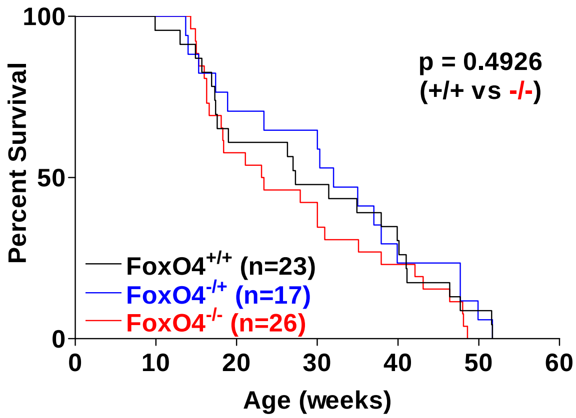

b

Tumor Type	FoxO4$^{+/+}$	FoxO4$^{-/+}$	FoxO4$^{-/-}$
Lymphoma	34.8% (8/23)	29.4% (5/17)	57.7% (15/26)
Lung adenoma/carcinoma	78.3% (18/23)	58.8% (10/17)	73.1% (19/26)
Skin papilloma	13% (3/23)	17.6% (3/17)	19.2% (5/26)
Angiosarcoma in Uterus (females)	0% (0/5)	17.6% (3/17)	15.4% (2/13)

c

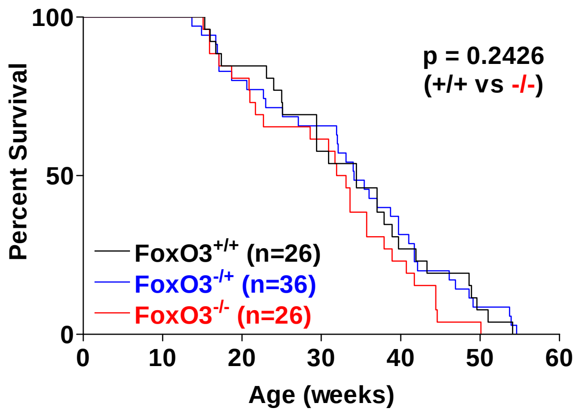

d

Tumor Type	FoxO3$^{+/+}$	FoxO3$^{-/+}$	FoxO3$^{-/-}$
Lymphoma	34.6% (9/26)	33.3% (12/36)	38.5% (10/26)
Lung adenoma/carcinoma	84.6% (22/26)	75% (27/36)	61.5% (16/26)
Skin papilloma	11.5% (3/26)	8.3% (3/36)	11.5% (3/26)
Angiosarcoma in uterus (females)	0% (0/14)	29.4% (5/17)	12.5% (1/8)

Figure S5.

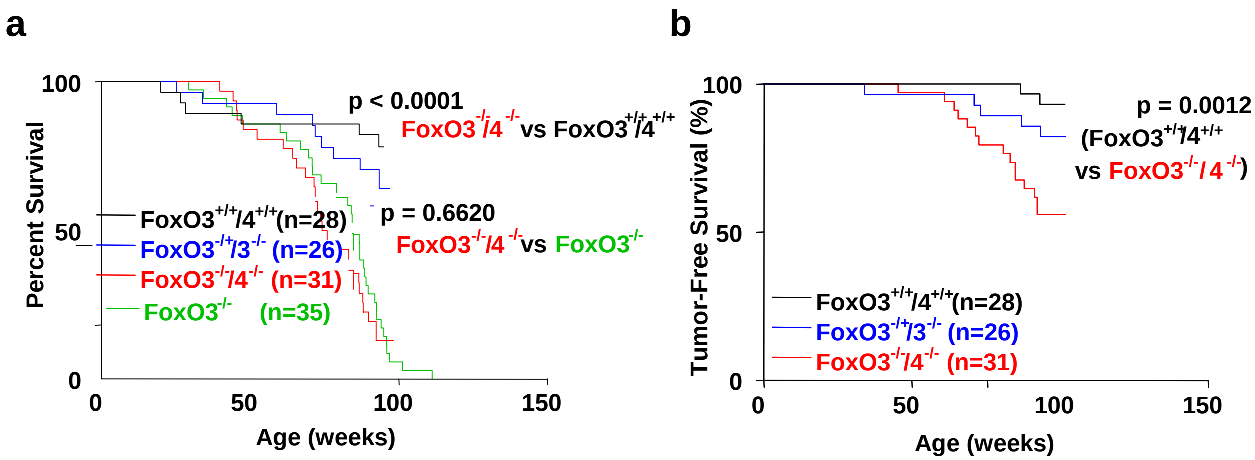

c

Tumor type	$FoxO3^{+/+}/4^{+/+}$	$FoxO3^{-/+}/4^{-/-}$	$FoxO3^{-/-}/4^{-/-}$
Lung adenoma/carcinoma	1/6 (16.7%)	1/9 (11.1%)	7/27 (25.9%)
Pituitary adenoma (females)	0	1/5 (20%)	6/13 (46.1%)
Pituitary adenoma (males)	0	0	0
Harderian gland adenoma	1/6 (16.7%)	2/9 (22.2%)	4/27 (14.8%)
Ovarian stromal neoplasm (females)	0	1/5 (20%)	1/13 (7.7%)
Cystic teratoma (ovary) (females)	0	0	2/13 (15.4%)
Other	0	1/9 (11.1%)	3/27 (11.1%)

Figure S6.

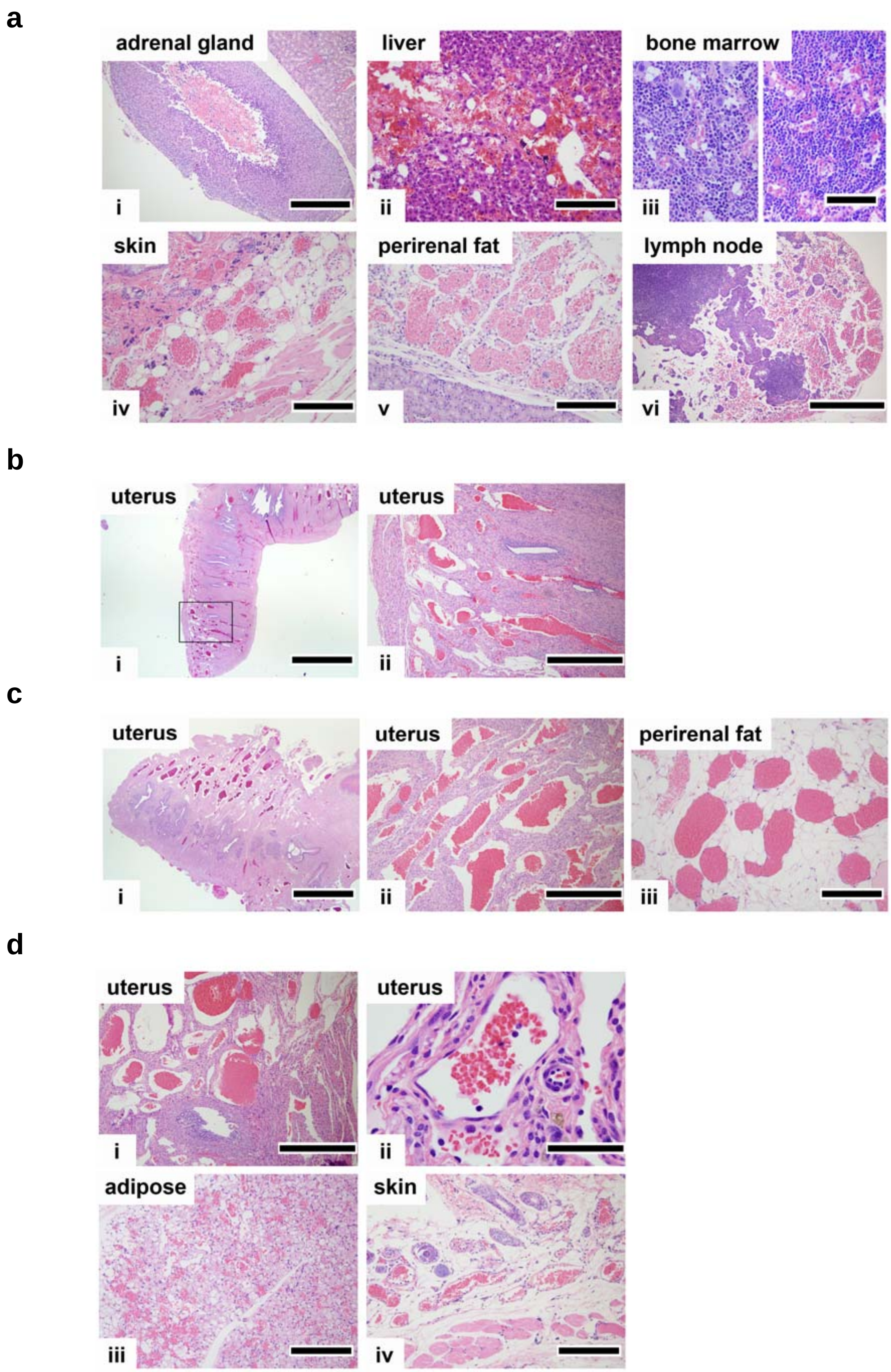
a
adrenal gland
i
liver
ii
bone marrow
iii
skin
iv
perirenal fat
v
lymph node
vi
b
uterus
i
uterus
ii
c
uterus
i
uterus
ii
perirenal fat
iii
d
uterus
i
uterus
ii
adipose
iii
skin
iv

Figure S7.

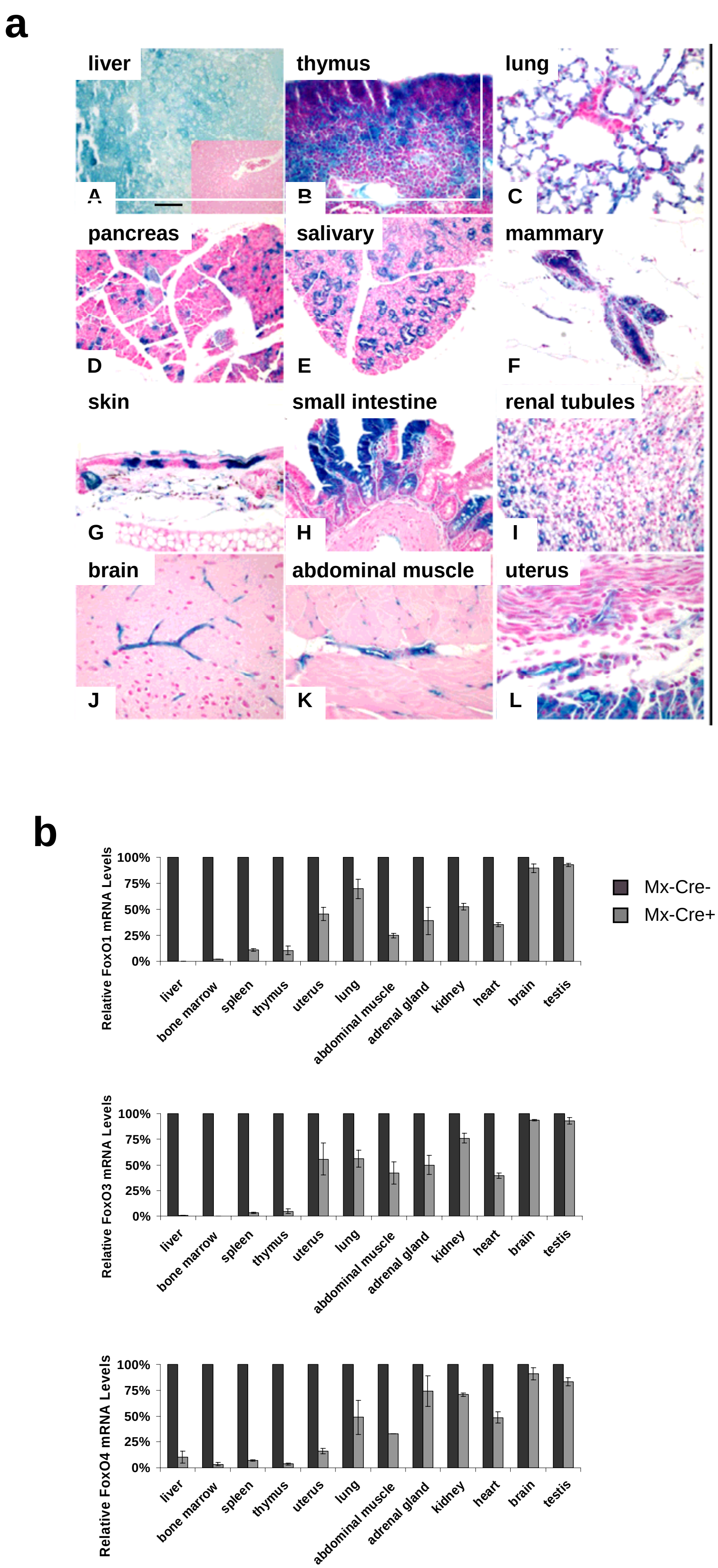
a
liver
thymus
lung
A
B
C
pancreas
salivary
mammary
D
E
F
skin
small intestine
renal tubules
G
H
I
brain
abdominal muscle
uterus
J
K
L
b
Relative FoxO1 mRNA Levels
100%
75%
50%
25%
0%
liver
bone marrow
spleen
thymus
uterus
lung
abdominal muscle
adrenal gland
kidney
heart
brain
testis
Mx-Cre-
Mx-Cre+
Relative FoxO3 mRNA Levels
Relative FoxO4 mRNA Levels

Figure S8.

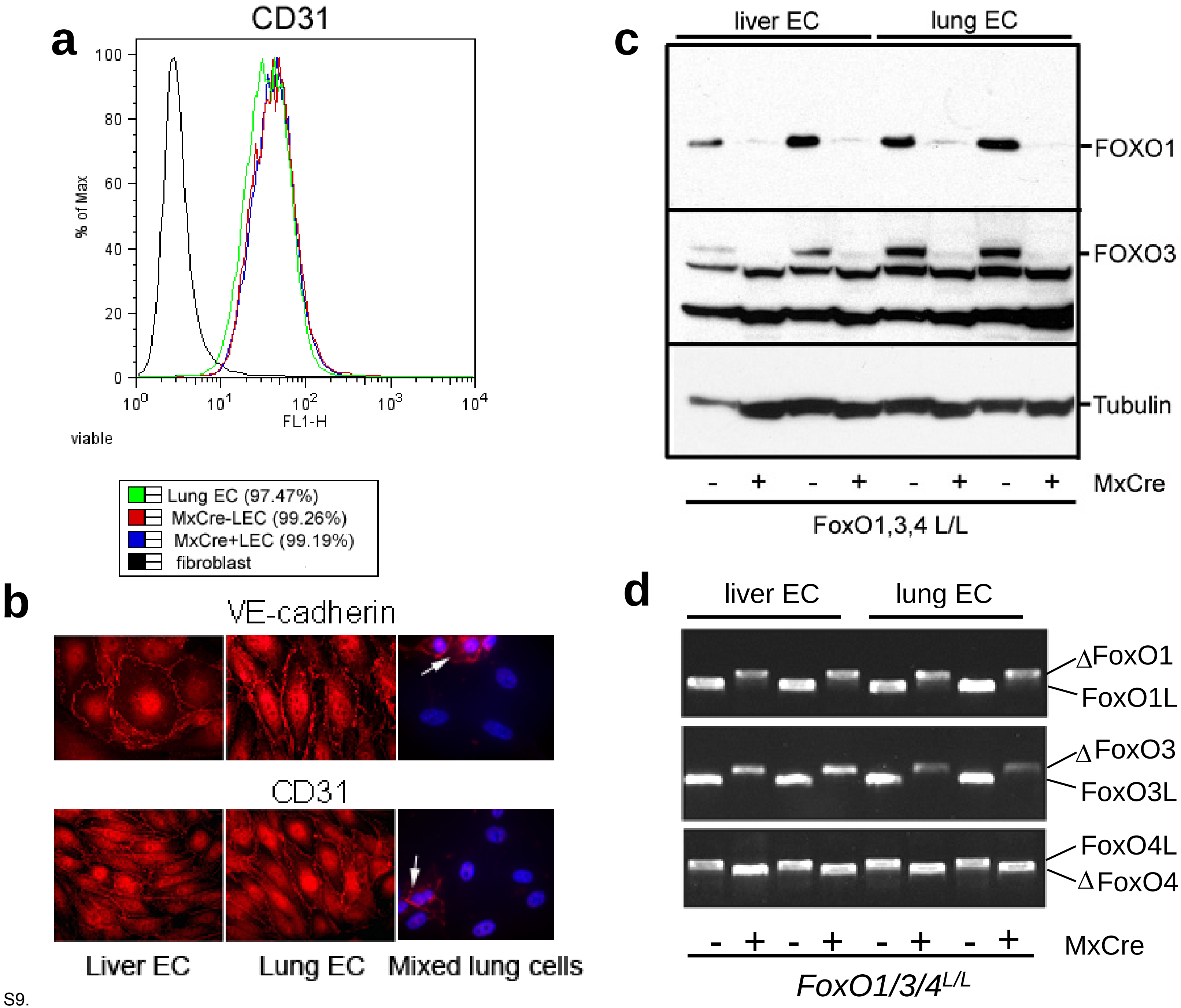
a
CD31
100
80
60
40
20
0
% of Max
10^0
10^1
10^2
10^3
10^4
FL1-H
viable
Lung EC (97.47%)
MxCre-LEC (99.26%)
MxCre+LEC (99.19%)
fibroblast
b
VE-cadherin
CD31
Liver EC
Lung EC
Mixed lung cells
c
liver EC
lung EC
FOXO1
FOXO3
Tubulin
- + - + - + - + MxCre
FoxO1,3,4 L/L
d
liver EC
lung EC
ΔFoxO1
FoxO1L
ΔFoxO3
FoxO3L
FoxO4L
ΔFoxO4
- + - + - + - + MxCre
FoxO1/3/4^L/L

Figure S9.

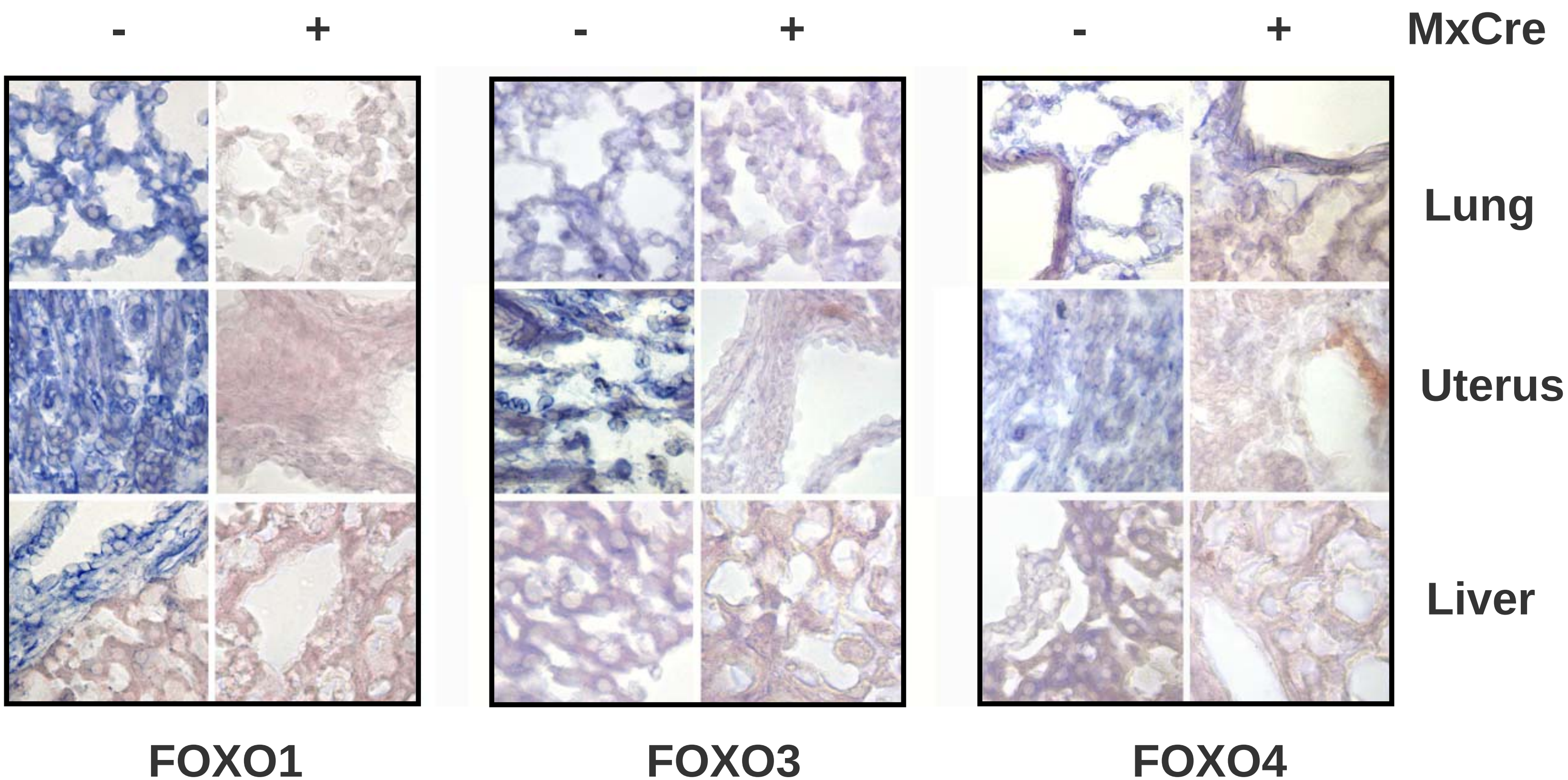

Figure S10.

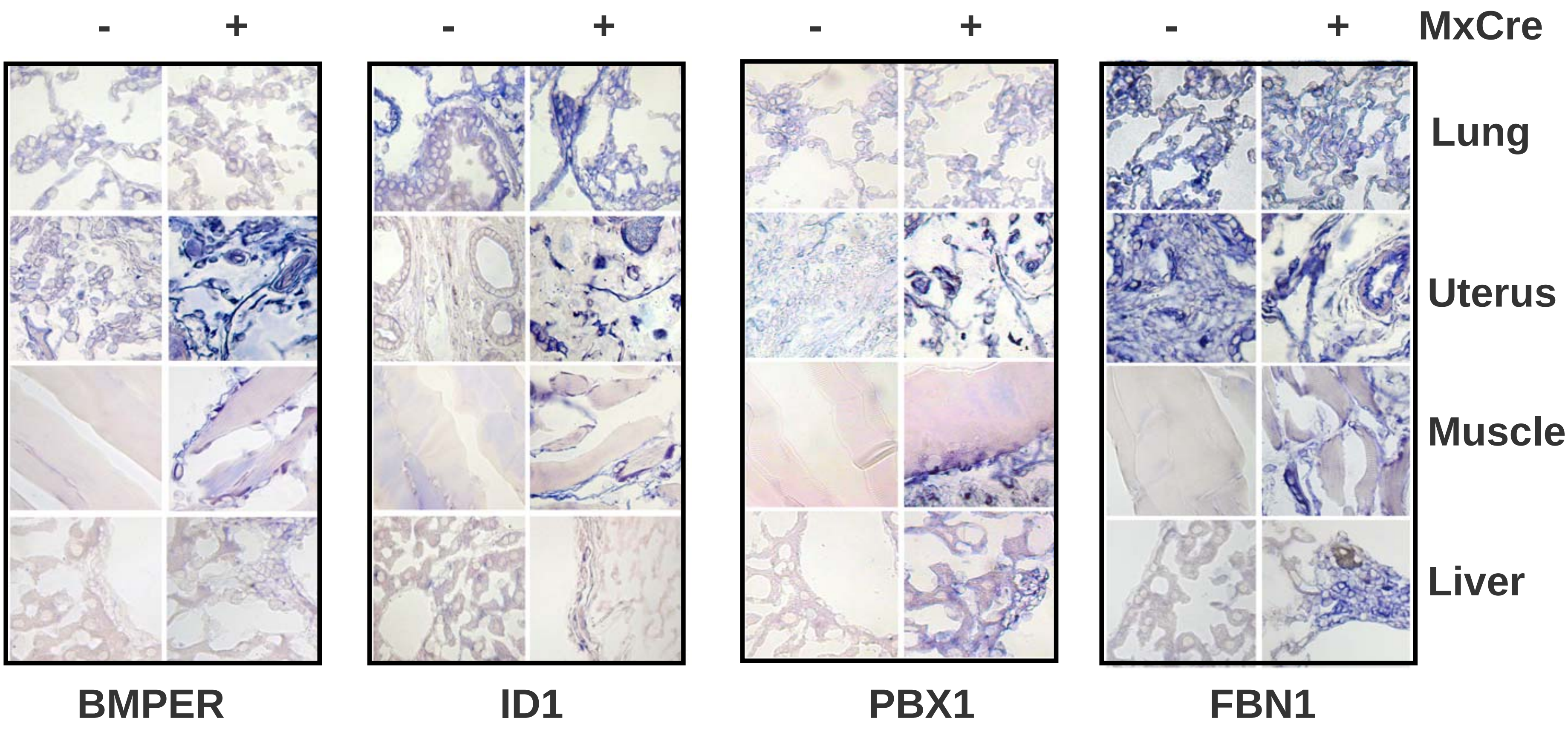

Figure S11.

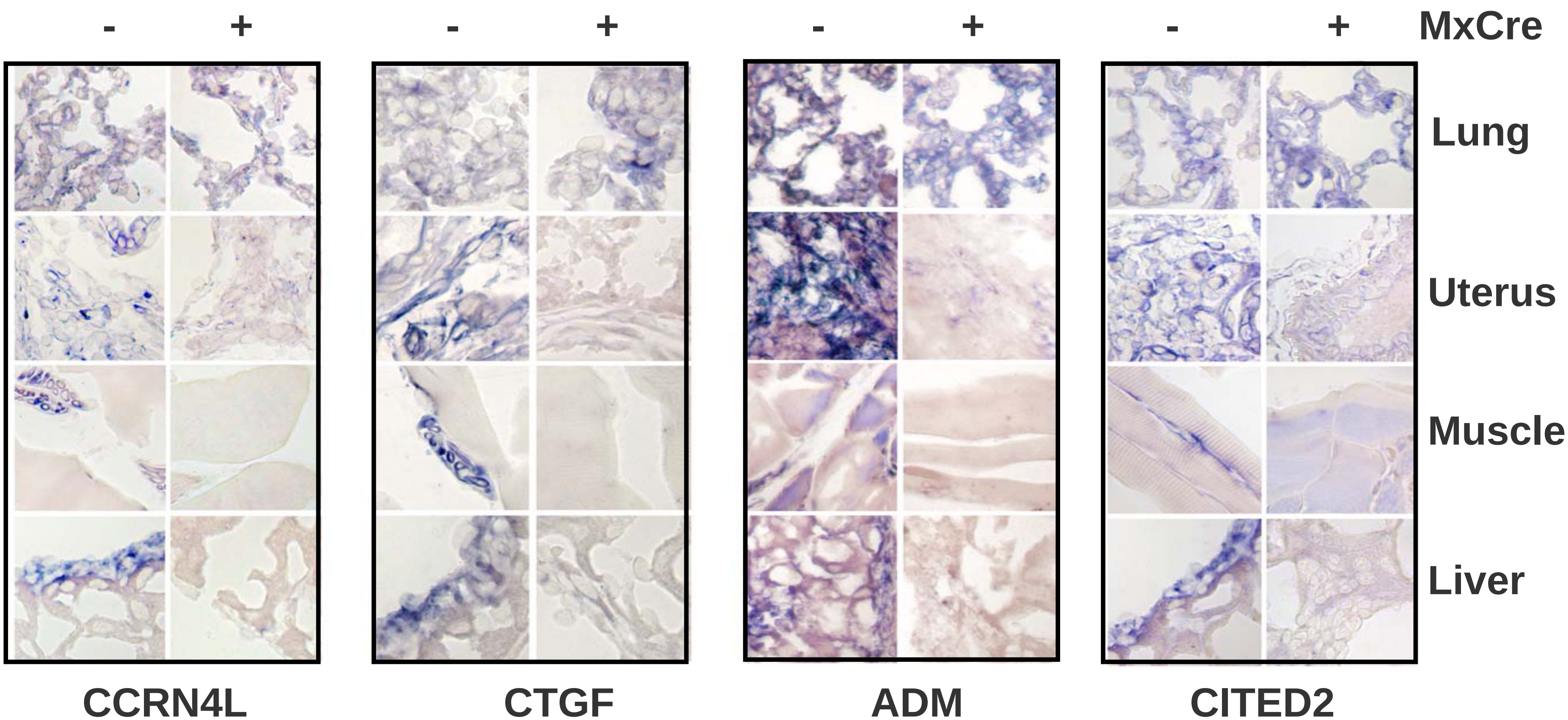

Figure S11.

Gene	5'	3'	direction	score	sequence	FoxO Binding by ChIP	primer/product
ADM	104482492	104482500	+	2.654504	CCTATTTTA	**YES**	**a**
	104482529	104482537	+	2.417648	GTTGTTTGG	NO	
	104485300	104485308	+	3.153852	GCTATTTTG	NO	
	104485795	104485803	+	3.102175	TTTGTTTTG		
	104486018	104486026	+	3.173715	GCTATTTTG	**YES**	**b**
CITED2	17642263	17642271	+	3.390792	CTTGTTTTG	**YES**	**c**
	17646180	17646188	-	2.569584	GTCGTTTTG	NO	
	17649093	17649101	+	2.628119	CTTGTTTCG	**YES**	**d**
	17649100	17649108	+	2.453474	CGTTTTTTG		
	17649172	17649180	+	2.760327	TTTGTTTTT		
	17651601	17651609	-	2.504161	CTTATTTTT	**YES**	**e**
	17652443	17652451	-	2.566627	CTTATTTTT		
	17653197	17653205	+	2.884156	CCTATTTTT		
CTGF	24569055	24569063	-	3.282897	TCTGTTTTG	**YES**	**f**
CCRNL4	50887258	50887266	-	3.042592	TCTATTTTG	**YES**	**g**
	50887724	50887732	+	2.513746	TTTGTTTTA	**YES**	**h**
	50887731	50887739	-	2.665946	GCTGTTTTA		
	50887785	50887793	-	3.153953	TTTGTTTTG		
BMPER	23114925	23114933	+	3.245308	TCTGTTTTG	**YES**	**I**
	23117308	23117316	+	2.793938	CTTATTTTT	**YES**	**j**
	23117378	23117386	+	2.979797	TCTATTTTG		
MRC1	14155565	14155573	+	3.089344	CCTGTTTTT	**YES**	**k**
PBX1	168089438	168089446	-	3.156608	TTTGTTTTG	NO	
	168089827	168089835	+	3.324043	CCTGTTTTG		
	168090150	168090158	-	2.534098	TTTATTTTT		
	168365064	168365072	-	3.041705	TCTGTTTTT	**YES**	**l**
	168365317	168365325	+	2.661249	TTTATTTTG		
	168365472	168365480	+	3.339045	CGTGTTTTT		
	168365708	168365716	-	3.012654	CTTGTTTTT		
	168367416	168367424	-	2.450942	TCGGTTTTT	**YES**	**m**

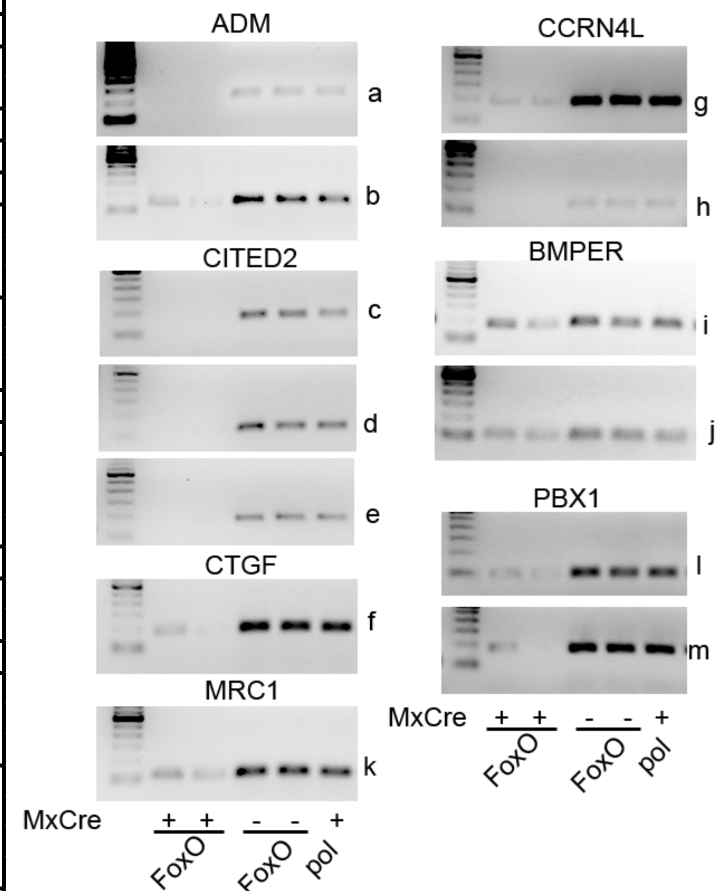

Figure S12.

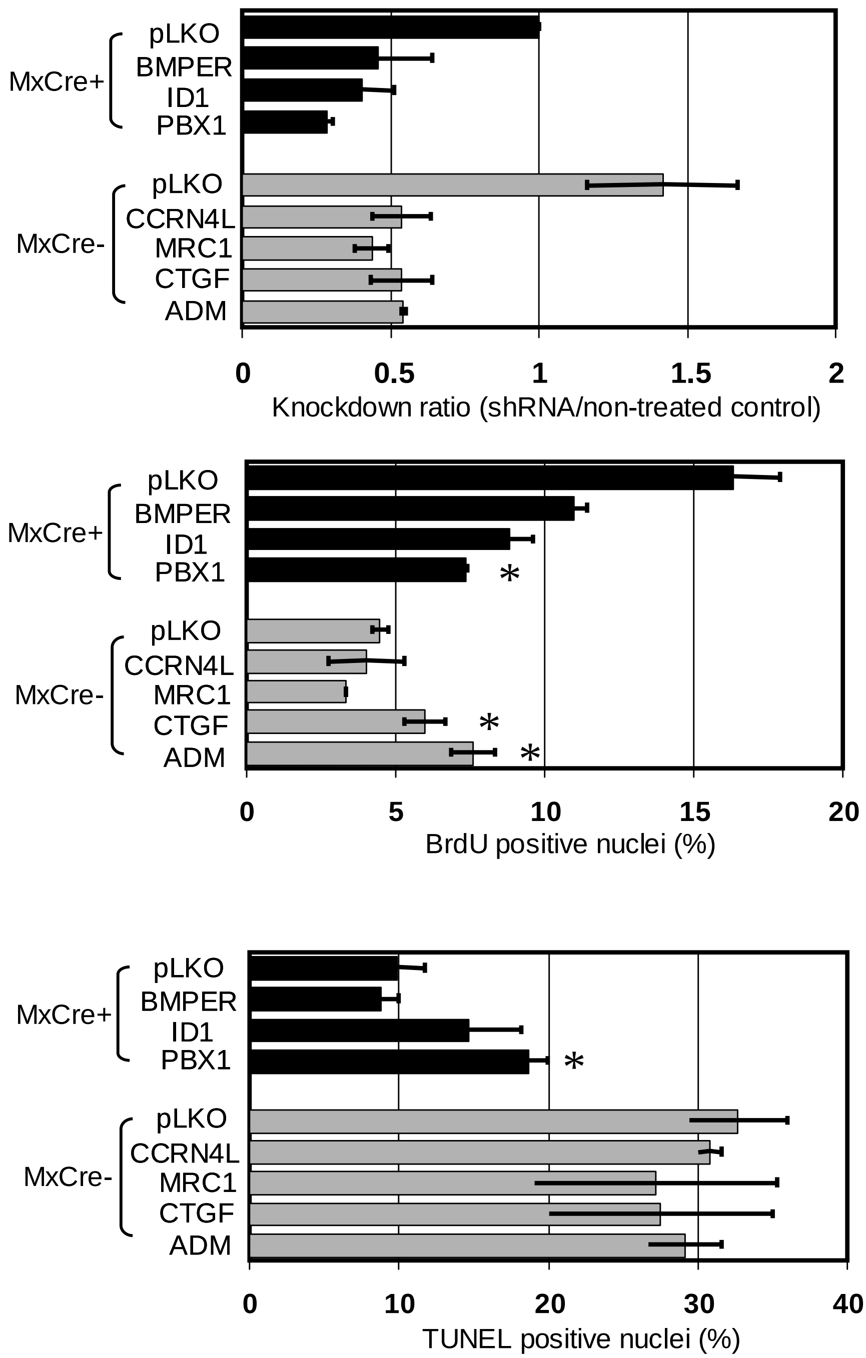
pLKO
BMPER
ID1
PBX1
MxCre+
pLKO
CCRN4L
MRC1
CTGF
ADM
MxCre-
0
0.5
1
1.5
2
Knockdown ratio (shRNA/non-treated control)
pLKO
BMPER
ID1
PBX1
MxCre+
pLKO
CCRN4L
MRC1
CTGF
ADM
MxCre-
0
5
10
15
20
BrdU positive nuclei (%)
pLKO
BMPER
ID1
PBX1
MxCre+
pLKO
CCRN4L
MRC1
CTGF
ADM
MxCre-
0
10
20
30
40
TUNEL positive nuclei (%)

Figure S13.

Supplementary Table S1: Tumor spectra of mice with germline mutation of a single FoxO gene

	Tumor Type	+/+	-/+	-/-
FoxO1	Lung adenoma/adenocarcinoma	11/31 (35/5%)	21/52 (40.4%)	
	Pituitary adenoma (females)	6/21 (28.6%)	4/29 (13.8%)	
	Pituitary adenoma (males)	1/10 (10%)	0	
	Hepatocellular carcinoma	2/31 (6.5%)	3/52 (5.8%)	
	Lymphoma	2/31 (6.5%)	1/52 (1.9%)	
	Hemangioma	0	1/52 (1.9%)	
	Angiolipoma	0	2/52 (3.8%)	
	Uterine Sarcoma NOS (females)	1/21 (4.8%)	1/29 (3.4%)	
	Sarcoma NOS	1/31 (3.2%)	1/52 (1.9%)	
	Breast carcinoma (females)	1/21 (4.8%)	1/29 (3.4%)	
	Other	0	5/52 (9.6%)	
FoxO4	Lung adenoma/adenocarcinoma	7/26 (26.9%)	5/15 (33.3%)	17/37 (45.9%)
	Pituitary adenoma (females)	0/11	2/15 (13.3%)	6/19 (31.6%)
	Pituitary adenoma (males)	0	0	0
	Breast carcinoma (females)	0	1/15 (6.7%)	2/19 (10.5%)
	Uterine sarcoma NOS (females)	3/11 (27.3%)	0	1/19 (5.2%)
	Hemangioma (in uterine horn)	1/26 (3.8%)	0	0
	Other	1/26 (3.8%)	0	4/37 (10.8%)
FoxO3	Lung adenoma/adenocarcinoma	11/22 (50%)	5/20 (25%)	8/35 (22.9%)
	Ovarian stromal tumor (females)	0	1/8 (12.5%)	4/16 (25%)
	Pituitary adenoma (females)	1/10 (10%)	1/8 (12.5%)	7/16 (43.8%)
	Pituitary adenoma (males)	0	0	0
	Harderian gland adenoma	2/22 (9.1%)	3/20 (15%)	2/35 (5.7%)
	Hepatocellular carcinoma	0	2/20 (10%)	1/35 (2.9%)
	Lymphoma	0	1/20 (5%)	3/35 (8.6%)
	Breast carcinoma (females)	2/10 (20%)	0	0
	Pheochromocytoma	1/22 (4.5%)	0	1/35 (2.9%)
	Hemangioma (in liver)	0	0	1/35 (2.9%)
	Other	3/22 (13.6%)	0	3/35 (8.6%)